Functional similarities between phage λ Orf and *Escherichia coli* RecFOR in initiation of genetic exchange

Karen L. Maxwell*†, Patricia Reed†‡, Rong-guang Zhang†§, Steven Beasley§, Adrian R. Walmsley‡, Fiona A. Curtis‡, Andrej Joachimiak§¶, Aled M. Edwards*, and Gary J. Sharples‡‖

‡Centre for Infectious Diseases, Wolfson Research Institute, University of Durham, Queen's Campus, Stockton-on-Tees TS17 6BH, United Kingdom; *Ontario Cancer Institute and Department of Medical Biophysics, University of Toronto, Toronto, ON, Canada M5G 2M9; §Midwest Center for Structural Genomics and Structural Biology, Argonne National Laboratory, 9700 South Cass Avenue, Argonne, IL 60440; and ¶Department of Biochemistry and Molecular Biology, University of Chicago, Chicago, IL 60637

Edited by Charles M. Radding, Yale University School of Medicine, New Haven, CT, and approved June 22, 2005 (received for review April 25, 2005)

Genetic recombination in bacteriophage λ relies on DNA end processing by Exo to expose 3′-tailed strands for annealing and exchange by β protein. Phage λ encodes an additional recombinase, Orf, which participates in the early stages of recombination by supplying a function equivalent to the *Escherichia coli* RecFOR complex. These host enzymes assist loading of the RecA strand exchange protein onto ssDNA coated with ssDNA-binding protein. In this study, we purified the Orf protein, analyzed its biochemical properties, and determined its crystal structure at 2.5 Å. The homodimeric Orf protein is arranged as a toroid with a shallow U-shaped cleft, lined with basic residues, running perpendicular to the central cavity. Orf binds DNA, favoring single-stranded over duplex and with no obvious preference for gapped, 3′-tailed, or 5′-tailed substrates. An interaction between Orf and ssDNA-binding protein was indicated by far Western analysis. The functional similarities between Orf and RecFOR are discussed in relation to the early steps of recombinational exchange and the interplay between phage and bacterial recombinases.

bacteriophage | DNA repair | genetic recombination | NinB

Genetic recombination in bacteriophages preserves genomic integrity by repairing strand breakages. However, exchanges occasionally occur at inappropriate sites, leading to rearrangement of existing genes or acquisition of new ones. Thus, considerable diversity is generated amongst phage populations, and this has a major impact on bacterial pathogen evolution by facilitating dissemination of virulence genes (1). The mechanism of phage recombination has been studied in some detail by using phage λ as a model system, partly as a consequence of its exploitation for *in vivo* genetic engineering (2). Two pathways of exchange predominate in λ depending on whether a DNA strand is used to invade a homologous duplex or is annealed to a complementary single-strand. Both envisage the restoration of a genomic dsDNA break by exchange with a second λ chromosome (3). The invasion reaction is typical of models for *Escherichia coli* recombination at a break and requires host RecA to bind ssDNA, locate a homologous duplex, and promote strand exchange to create a recombinant joint (4). The second pathway functions independently of RecA and involves annealing of homologous ssDNA partner sequences. This reaction requires the breaks to be located at different sites in separate λ genomes and depends on the annealing properties of phage β protein (3, 5). Recombination in both reaction pathways is initiated by the coupled action of phage Exo and β proteins, collectively termed the Red system (2, 5). Exo is a 26-kDa exonuclease, degrading ssDNA in the 5′ to 3′ direction from a duplex DNA end to produce 3′ overhangs (6). The 30-kDa β protein can generate recombinants by annealing the 3′-tailed product generated by Exo to complementary ssDNA sequences (3, 7, 8). Recent experiments suggest that β can also perform strand invasion reactions similar to those mediated by RecA (9).

In addition to Exo and β, λ encodes a third protein, Orf (NinB), which is influential in the initial phase of genetic exchange (10–12). The 17-kDa Orf substitutes for a complex of three *E. coli* proteins (RecF, RecO, and RecR) in λ *red* mutant crosses but not during host conjugational exchange (10, 11). However, Orf can replace *recFOR* function in *E. coli* recombination when Exo and β are present (12). Mutations in any of the *recFOR* genes normally confer modest deficiencies in DNA repair and recombination, phenotypes that can be partially suppressed by RecA mutations improving its ability to nucleate on ssDNA and displace ssDNA-binding (SSB) protein (13, 14). Individually and corporately, RecFOR exhibit a remarkable array of *in vitro* activities. RecF binds ssDNA or dsDNA and possesses a weak ATPase activity important in dissociation from dsDNA (15–17). RecO binds DNA and promotes strand invasion and annealing of homologous sequences, especially those already bound by SSB (18–20). The monomeric RecO is composed of three domains: an N-terminal oligonucleotide/oligosaccharide binding fold, a central α-helical bundle, and a C-terminal zinc-binding motif (21). RecR proteins from *Bacillus subtilis* and *Deinococcus radiodurans* bind DNA (22, 23), although *E. coli* RecR apparently does not (16, 24). Four RecR subunits are arranged as a toroid with a central hole of 30–35 Å in diameter, which probably accommodates dsDNA (23). There is evidence for RecFO, RecFR, RecOR, and RecFOR interactions and an association between RecO and SSB (24–26). RecFR limits extension of RecA on duplex DNA after initial filament assembly on ssDNA, whereas RecOR helps RecA gain access to ssDNA blocked by the presence of SSB protein (27). All three together are required to load RecA at ssDNA–dsDNA junctions containing a 5′ end when SSB coats ssDNA at gaps (28). Finally, RecFOR appears to safeguard the nascent strands at stalled replication forks (29) and is toxic in certain mutant backgrounds where DNA replication is impaired, suggesting that inappropriate loading of RecA at replication forks is detrimental to survival (30, 31).

To elucidate how a single phage protein, Orf, can substitute for three much larger host polypeptides, we purified λ Orf, determined its crystal structure, and characterized its interactions with DNA substrates designed to mimic the early inter-

This paper was submitted directly (Track II) to the PNAS office.

Abbreviations: SSB, ssDNA-binding protein; MBP, maltose-binding protein.

Data deposition: The atomic coordinates have been deposited in the Protein Data Bank, www.pdb.org (PDB ID code 1PC6).

†K.L.M., P.R., and R.-g.Z. contributed equally to this work.

‖To whom correspondence should be addressed. E-mail: gary.sharples@durham.ac.uk.

mediates of genetic recombination. A physical interaction between Orf and SSB suggests that the λ protein fulfils an important role in helping recombinases gain access to the DNA template, a function conserved throughout biology.

Materials and Methods

Purification of Orf Protein for DNA-Binding Analysis. The *orf* (*ninB*) gene was amplified by PCR from λ genomic DNA and inserted into pET14b (pPR100) or pET15b (pKM123) to generate an N-terminal His_6 affinity tag fusion containing a thrombin cleavage site. The integrity of the cloned *orf* gene from both constructs was confirmed by DNA sequencing. Orf was overexpressed from 2 liters of *E. coli* BL21 pLysS carrying pPR100 and purified on nickel-iminodiacetic acid Sepharose and heparin agarose columns (Sigma). Orf was stored in 20 mM Tris·HCl, pH 8.0/1 mM EDTA/0.5 mM DTT/500 mM KCl/50% glycerol at −80°C. A total of 2.6 mg of purified Orf was recovered at 1.3 mg/ml. Protein concentrations were determined by a modified Bradford Assay (Bio-Rad) using BSA as a standard; amounts of protein are expressed as moles of dimeric protein.

Orf Sample Preparation for Crystallography. *E. coli* BL21-Gold cells carrying pKM123 were grown at 37°C in TB medium supplemented with 4% glucose to an A_{600} of 1.0. Protein expression was induced with 1 mM IPTG, followed by 4 h incubation at 37°C. Orf was purified and prepared for crystallization studies as described (32). As a final purification step, gel filtration was performed by FPLC on a 25-ml Superdex-75 column (Amersham Pharmacia). Fractions containing pure protein as assayed by SDS/PAGE were concentrated by ultrafiltration. Selenomethionine-enriched Orf was expressed in the methionine auxotroph *E. coli* B834(DE3) in supplemented M9 medium and was purified as the native protein, except 5 mM 2-mercaptoethanol was added to the purification buffers.

Crystallization of Orf. Orf crystals were obtained by vapor diffusion in hanging drops (3 μl of protein to 3 μl of precipitant) over 1.4 M sodium acetate/0.05 M sodium cacodylate, pH 6.9, for 2–4 days at 21°C. For diffraction studies, the crystals were flash-frozen with the crystallization buffer plus 25% ethylene glycol. The crystals formed hexagonal rods reaching dimensions of 500 × 150 × 150 μm and belong to trigonal space group $P3_2\,2\,1$, with unit cell dimensions $a = b = 76.78$ Å, and $c = 107.39$ Å.

Crystal Structure Determination. Diffraction data were collected at 100K at the 19ID beamline of the Advanced Photon Source (Argonne National Laboratory) as described (33). The three-wavelength anomalous diffraction (MAD) data (peak, 0.9795 Å; inflection point, 0.9797 Å; high remote, 0.94656 Å) were collected to 2.5 Å from the selenomethionine-substituted protein crystal by using an inverse-beam strategy. All data were processed and scaled by using HKL2000 (34). Patterson searches, MAD phasing, density modification, initial map calculation, and structure refinement were carried out by using the CNS suite (35). The initial model was built automatically by using ARPWARP (36), and consists of 75% main chain and 45% side chains. The model was rebuilt manually by using QUANTA and improved through several cycles of refinement and model building. The final model was refined to 2.50 Å by using CNS against the peak data. The final *R*-factor was 0.234, and the R_{free} was 0.294.

DNA Substrates. Oligonucleotides used are listed in Table 1, which is published as supporting information on the PNAS web site. For band shift assays, one oligonucleotide was labeled with [γ-^{32}P]ATP at its 5′ end by using T4 polynucleotide kinase.

DNA-Binding Assays. Band shift assays using ^{32}P-labeled DNA substrates were performed in 50 mM Tris·HCl, pH 8.0/5 mM EDTA/1 mM DTT/5% glycerol/100 μg/ml BSA. Samples were incubated on ice for 15 min before separation on 4% PAGE in 6.7 mM Tris·HCl, pH 8.0/3.3 mM sodium acetate/2 mM EDTA. Gels were dried onto filter paper and analyzed by autoradiography and PhosphorImaging. The interaction between Orf and DNA was time-resolved on an Applied Photophysics SX.18MV stopped-flow instrument. For measurements of the change in tryptophan fluorescence, samples were excited with light at 285 nm, selected with a monochromator, and emission monitored at wavelengths >335 nm by using a cutoff filter. Routinely, equal volumes of the reactants were mixed together in the stopped-flow instrument. To set up the instrument, 1.25 μM Orf protein was mixed with 50 mM Tris·HCl (pH 8.0), and the photomultiplier tube voltage was increased to 4 V and then backed-off to zero, and changes about this zero baseline recorded.

Far Western Blotting. SSB protein was purified as described (37) apart from omission of the gel-filtration step. An N-terminal maltose-binding protein (MBP)–Orf fusion expressed from pMALc2 was purified on amylose resin. SSB was separated on SDS/15% PAGE and transferred to poly(vinylidene difluoride) membrane by electroblotting in 10 mM cyclohexylaminopropanesulfonic acid/20% methanol. A prestained protein molecular weight standard served as a size marker. Blots were probed with MBP–Orf protein, and interactions were detected with monoclonal anti-MBP antibodies and mouse IgG peroxidase conjugate (Sigma). Chemiluminescence was observed by exposure to x-ray film after treatment with enhanced chemiluminescence reagents (Amersham Pharmacia).

Results and Discussion

Interaction of Orf with DNA. The λ *orf* gene was cloned into pET expression vectors and purified as an N–His_6 fusion by nickel-affinity chromatography followed by further fractionation on heparin agarose. Because all three components of the RecFOR complex show some association with DNA, we investigated the ability of Orf to bind different DNA substrates in gel mobility-shift assays. Orf formed at least two discrete complexes with a 50-nt DNA substrate, but bound much less well to a duplex of the same sequence (Fig. 1*A*). The obvious band smearing with the duplex indicates that Orf forms an unstable association with dsDNA (Fig. 1*A*, lane h). A clear preference for binding ssDNA was evident when a larger range of protein concentration was used (Fig. 1*B*). Samples of Orf protein lacking the N-terminal tag gave very similar DNA binding profiles on these two substrates (data not shown).

To further probe the interaction of Orf with DNA, we used stopped-flow fluorescence spectroscopy. This approach can be used to evaluate interactions between proteins and their substrates assuming an appropriately situated tryptophan residue is available and is sufficiently close to the ligand binding site. Orf contains seven tryptophans, and the fluorescence of one or more of these is quenched when protein and DNA are mixed on a stopped-flow device (Fig. 2*A*). The fluorescence decrease is most likely a consequence of DNA blocking the exposed tryptophan(s) or a conformational change in protein architecture resulting in burying of these residues. The rate and differences in amplitude of the fluorescence quench show that Orf binds to ssDNA (either 25 or 50 nt) in preference to dsDNA of the same length and sequence (Fig. 2*A*). Binding of Orf to ssDNA appears to occur in two phases with a rapid initial quench in fluorescence followed by a slower change between 10 and 30 s. Very similar binding profiles were obtained by using a 50-base oligonucleotide containing a 25-bp duplex section at either the 5′ or 3′ end, or in the center of the molecule (Fig. 2*B*, see Fig. 5*B*). Thus, Orf does not appear to favor loading at the intersection between single- and double-stranded DNA as noted with RecF (38) and RecFOR (28).

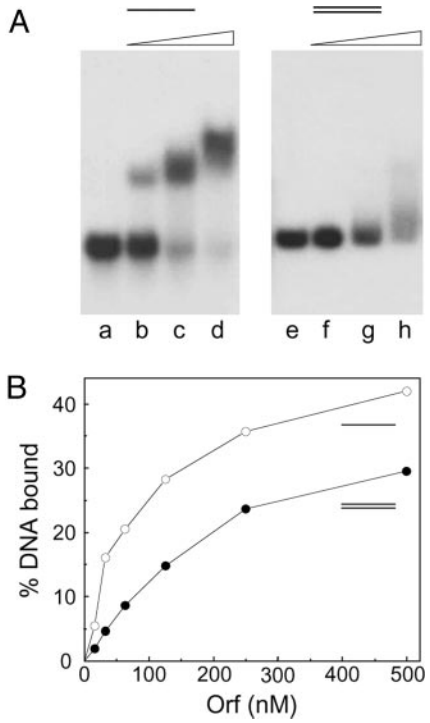

Fig. 1. Orf binding to DNA in gel mobility shift assays. (*A*) Samples contained 0.3 nM ssDNA (lanes a–d) or dsDNA (lanes e–h) with 0, 5, 50, and 500 nM His–Orf protein. (*B*) Binding reactions contained 0.3 nM ssDNA and dsDNA as indicated with 0, 15.625, 31.25, 62.5, 125, 250, and 500 nM His–Orf. Data are the mean of two independent experiments.

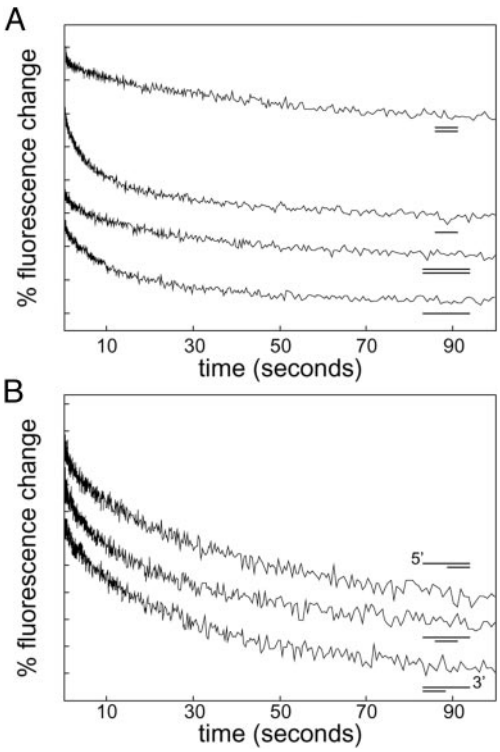

Fig. 2. Orf binding to DNA in stopped-flow assays. Samples were mixed on the stopped-flow instrument to give final concentrations of 625 nM His–Orf and 5 μM DNA as indicated. (*A*) Binding to 25- and 50-mer ssDNA and dsDNA substrates. (*B*) Binding to 50-mer 5′ and 3′ overhangs and tailed duplex DNA substrates. Each division on the *y* axis represents a fluorescence change of 5% (*A*) and 2% (*B*).

One of the components of the RecFOR complex, RecO, has the capacity to anneal homologous single-stranded DNA molecules (18, 20), and so we assayed Orf for strand annealing activity. Using polyacrylamide gels to monitor duplex formation of ^{32}P-labeled DNA, we found no evidence that Orf could anneal either homologous oligonucleotides (50 nt) or those (25 and 50 nt) matching ϕX174 circular ssDNA. Similarly, Orf failed to stimulate strand annealing in stopped-flow assays using DAPI to quantify formation of dsDNA from oligonucleotide pairs (data not shown). Because λ β is a single-strand annealing protein (7, 8), it is perhaps unsurprising that Orf lacks this activity. Nevertheless, the ssDNA-binding properties of Orf clearly correlate with its predicted role in initiation of exchange at gaps or ends where β and RecA compete with SSB for access.

Crystal Structure of Orf Protein. To help ascertain how Orf interacts with DNA, we determined its atomic structure by x-ray crystallography using multiwavelength anomalous diffraction data from a single crystal of selenomethionine-substituted protein. Statistics describing the quality of x-ray diffraction data are summarized in Table 2, which is published as supporting information on the PNAS web site. There are two 146-residue chains in the asymmetric unit; the final model includes residues 1–141 for chain A, and 1–133 for chain B. The Ramachandran plot produced by PROCHECK (39) shows that, of 274 residues in the model, 88.1% are in the most favored regions, 11.1% are in additional allowed regions, and no residues fall in the disallowed regions. Statistics related to the final refined protein model are shown in Table 3, which is published as supporting information on the PNAS web site.

The 2.51-Å resolution structure reveals that Orf belongs to the $\alpha + \beta$ protein class, and possesses a unique fold as determined by the DALI algorithm (40). Two Orf monomers are arranged as an intertwined dimer, forming a ring with a funnel-like channel through the center (Fig. 3 *A* and *B*). The Orf structure can be loosely divided into two components: a larger C-terminal region, composed of two three-helix bundles and two antiparallel β-sheets, and a smaller N-terminal region comprising a single antiparallel β-sheet topped by two α-helices. Each Orf monomer consists of two separate regions that interact to form the oligomeric structure (Fig. 3*C*). The first region comprises the initial 38 residues of the protein and includes three segments that contribute to the dimer interface: residues 3–9 (β1), 14–22 (αA), and 26–38 (β2 loop and β2). The β-strands form a single intertwined β-sheet, and the two α-helices pack across the top of the β-sheet in a parallel manner. The second region comprises residues 67–97, and also has three segments contributing to the interface: residues 67–80 (αC), 83–89 (β3), and 95–97 (β4). In this region, the α-helix of one monomer packs on top of an antiparallel β-sheet formed by the two strands from the other monomer. Nine hydrophobic residues from each monomer (Ile-8, Val-21, Val-33, Ile-36, Val-75, Val-86, Leu-89, Val-95, and Ile-97) are highly buried in the dimer interface. With the exception of Val-33, the hydrophobic character of each of these residues is highly conserved between Orf homologs (Fig. 3*D*). There are also six salt bridges and numerous ionic interactions mediated through water molecules that contribute to the stability and specificity of the dimer interface. The size of the oligomeric interface (1,407 Å^2 buried per subunit) is close to the average of 1,700 $\pm$ 1,100 Å^2 observed for homodimers (41), and accounts for $\approx$20% of the accessible surface of each subunit. To investigate the role of the dimer conformation in the crystal structure, size exclusion chromatography and cross-linking experiments were performed. The homogenous Orf protein preparation formed an apparent dimer of 33 kDa on size exclusion chromatography and when exposed to the cross-linking agent glutaral-

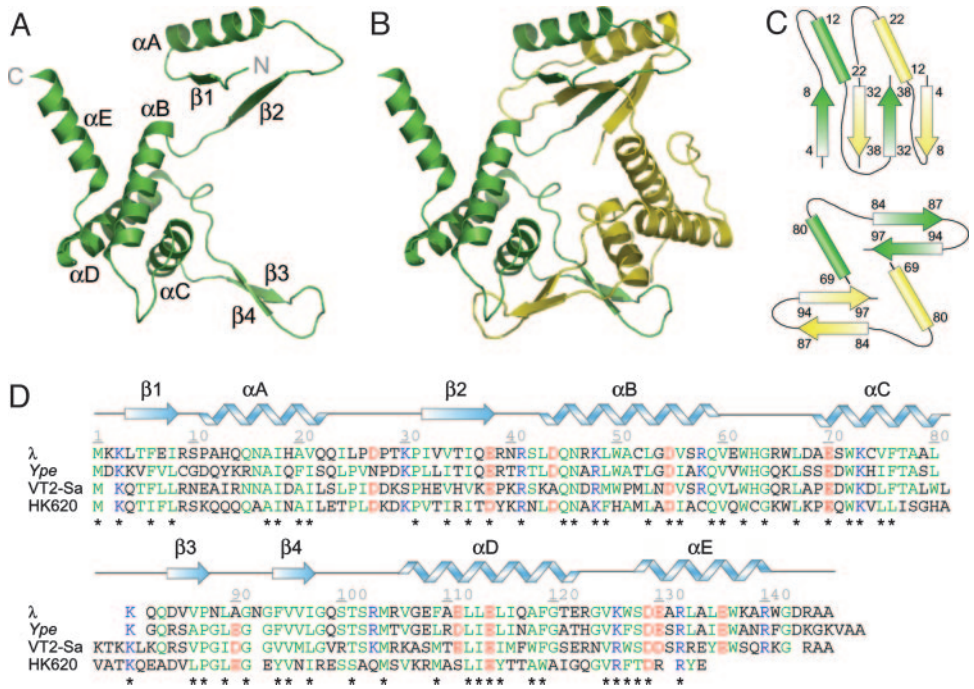

Fig. 3. Primary, secondary, and tertiary structure of Orf. (*A*) Ribbon diagram of an Orf subunit with secondary structure elements labeled. (*B*) Overall view of the dimeric structure of Orf with monomer A shown in green, and monomer B in yellow. (*C*) Schematic representation of the N- and C-terminal dimerization regions of Orf. The strands and helices are colored as in *B*. (*D*) Sequence alignment of selected phage Orf homologs. Conserved residues are highlighted: acidic (red), basic (blue), and others (green). Asterisks denote residues conserved in all four sequences. The representative homologs come from a *Yersinia pestis* prophage (*Ype*), *E. coli* O157:H7 phage VT2-Sa, and *E. coli* H phage HK620. Secondary structure elements are indicated above the residue numbers given for the λ Orf sequence.

dehyde (Fig. 7, which is published as supporting information on the PNAS web site).

The Orf dimer exhibits asymmetry due to a twist in the backbone at residues Asn-40–Ser-42. When the two monomers are examined, residues Lys-3–Glu-38 can be aligned with an rms deviation (rmsd) of 0.78 Å over 144 backbone atoms, and residues Ser-42–Ser-128 can be aligned with an rmsd of 0.65 Å over 352 backbone atoms. The hinge point involves residues Asn-40 and Arg-41, which have ϕ/ψ angles of $-104/-45.5$ and $-117/124$, respectively, in monomer A and $-47/150$ and $-43/-57$, respectively, in monomer B. Additional asymmetry is provided by the C-terminal tail, which extends away from the protein out into solution. After the fourth α-helix (residues 106–121), monomer A has an α-helix comprised of residues 128–140, whereas monomer B has random coil until residue 133, when the electron density is missing, indicating that this region is disordered. Examination of the crystal data shows that the C terminus of monomer A packs against three neighboring proteins in the crystal, stabilizing αE. The extended conformation of the helix in monomer A and disorder observed at the C terminus of monomer B suggests that the last 20 residues are flexible and could adopt different conformations in Orf complexed to DNA or other proteins. There are several reports in the literature of asymmetry in homodimer–nucleic acid interactions, including nonstructural protein B (NSP3) from Rotavirus, which forms a heart-shaped, asymmetric homodimer when bound to RNA, creating a single RNA-binding site (42). The HIV-1 reverse transcriptase also forms an asymmetric dimer, creating only one RNA-dependent DNA polymerase active site, one RNase H active site, one tRNA-binding site, and one noncompetitive inhibitor-binding site (43). A similar situation may arise in the Orf dimer, allowing it to interact with DNA as well as providing binding sites for other recombinases.

Calculation of the molecular surface of the protein performed by the program SPOCK (http://quorum.tamu.edu) reveals a central channel that traverses the dimer (Fig. 4*A*). Electrostatic calculations show that the interior of this channel is very positively charged (Fig. 4*B*), due to several highly conserved residues (Lys3A/B, Arg41A, Lys73A/B, and Lys81A; Fig. 3*D*). The channel ranges in diameter from ≈20 Å at the top to only 8 Å near the bottom, and could potentially accommodate the passage of ssDNA like a bead on a string. The distal end of the cavity is partially occluded by the first two residues of monomer B. However, the presence of either a polyhistidine or maltose-binding protein tag at the N terminus had no significant impact on Orf DNA binding activity (data not shown), suggesting that either DNA does not pass through this channel, or that the N terminus of monomer B is able to change conformation to accommodate it. Alternatively, binding to ssDNA could occur within a shallow U-shaped cleft that traverses the top of the central opening and is lined with a number of positively charged residues (Fig. 4*C*). In addition, the aromatic residue Trp50A is also present in the putative DNA binding region, and could act to stabilize the ssDNA–protein complex by stacking against the nucleotide bases.

Binding to ssDNA Across the Surface Cleft. To determine whether Orf threads ssDNA through the central cavity or across the surface cleft, we examined binding to a gapped duplex substrate based on the premise that dsDNA would be unable to penetrate the narrow aperture. We used a 26-nt stretch of ssDNA flanked at each end by 17-bp duplexes. Orf readily binds 25-mer oligonucleotides (Fig. 2*B*), so this gapped region should be sufficiently large to accommodate at least one Orf dimer. Control tailed substrates were made by simply omitting either of the short strands making up the duplex sections. In band shift assays with ^{32}P-radiolabeled DNA, Orf bound to all three of the substrates with similar affinities (Fig. 5*A*), indicating that ssDNA is ac-

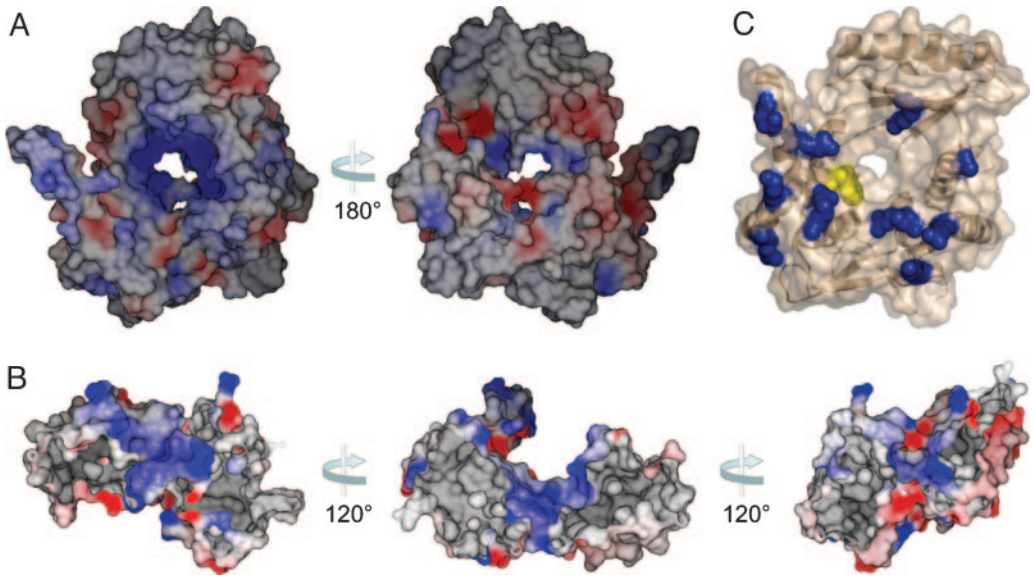

Fig. 4. Potential Orf DNA-binding sites. (*A*) Electrostatic surface representation of chemical properties of the solvent accessible surface of the Orf dimer calculated by using a probe radius of 1.4 Å. The surface is colored red and blue, representing electrostatic potentials less than −20 *kBT*, or greater than +20 *kBT*, where *B* is the Boltzman coefficient and *T* is temperature. A view of the potential DNA binding site looking through the central channel from the top (*Left*) and bottom (*Right*) of the protein is shown. (*B*) This view is rotated by 90° about the *x* axis from *A*. The front half of the protein is removed to show the contours and electrostatic charge present in the interior of the channel that runs the length of the protein. Each of the three representations are rotated about the *y* axis by 120°. (*C*) Molecular surface representation illustrating the potential DNA binding cleft that traverses the top of the Orf dimer. Basic residues are shown in blue, Trp50A is shown in yellow.

commodated within the surface cleft. Binding to the gapped duplex was also monitored by stopped-flow spectroscopy (Fig. 5*B*). Very similar fluorescence change profiles were detected by using the gapped duplex, ssDNA, or 5′ and 3′ overhangs (Fig. 5*B*), implying that Orf binds each of these substrates equally well. At this concentration of DNA, very little decrease in protein fluorescence was detected with dsDNA. Taken together, the data suggest that ssDNA is accommodated within the U-shaped cleft of Orf rather than passing through the central channel of the ring (Fig. 4). This finding fits with the ability of Orf to associate with both ssDNA and dsDNA, albeit weakly with the latter.

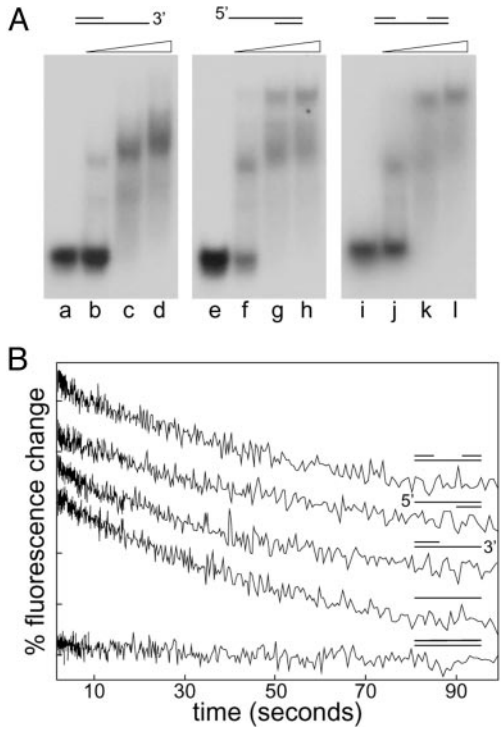

Fig. 5. Defining the Orf DNA-binding site. (*A*) Gel-shift assays of binding to 0.3 nM 60-mer 3′ overhang (lanes a–d), 5′ overhang (lanes e–h), and gapped duplex (lanes i–l) with His–Orf protein at 0, 5, 50, and 500 nM. (*B*) Stopped-flow assays of His–Orf (625 nM) binding to DNA (0.5 μM). Each division on the *y* axis represents a fluorescence change of 5%.

Orf and SSB Interact. RecFOR promote assembly of RecA filaments on SSB-coated DNA (28). Therefore, we investigated

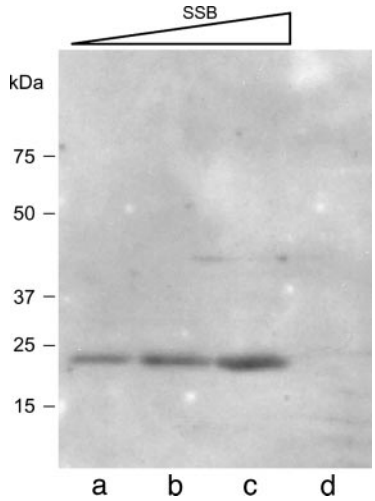

Fig. 6. Interaction between Orf and SSB. Far Western analysis on purified SSB (lanes a–c) at 0.5, 1.9, and 3.8 μg separated on SDS/15% PAGE. Lane d contained no protein. Blotted SSB protein was probed with 20 μg of MBP–Orf and interactions detected with anti-MBP antibodies.

whether Orf could interact directly with SSB by using far Western blotting. Wild-type SSB protein on a poly(vinylidene difluoride) membrane was probed with purified MBP–Orf and antibodies directed against the tag. The 19-kDa SSB protein was detected in purified (Fig. 6) and overexpressed samples, indicating that Orf and SSB interact. Similar results were obtained by using MBP–Orf on gels with purified His–SSB as a probe with anti-His antibodies. No signal was detected in the absence of MBP–Orf protein or using MBP alone (data not shown).

Potential Function of Orf in Initiation of Genetic Exchange. The *in vitro* ssDNA and SSB binding properties of Orf clearly fit with a role in the initial steps of genetic exchange as predicted by its ability to substitute for RecFOR in recombination reactions *in vivo* (10, 12). As with the RecFOR complex, Orf could aid RecA nucleation on ssDNA prebound by SSB (12), although why a phage system should mimic so closely that of its host is unclear. It is possible, because Orf shows no apparent preference for the 5′ ended structure recognized by RecFOR (28), that loading RecA onto any available ssDNA has specific advantages for phage recombination. Alternatively, Orf could encourage loading of β protein to overcome the inhibitory presence of SSB; this may explain why Orf seems to function better in recombination reactions mediated by the Red system (12) rather than those supported by its host (11). It has always been assumed that Exo aids loading of β onto ssDNA during end degradation, because the two recombinases are known to form a complex (2). Orf may be needed to help β gain access to ssDNA in other situations, for example those exchanges occurring at gaps or replication forks (44). The fluorescence quench observed when Orf associates with DNA could indicate a conformational change that helps either displace SSB or allows access of RecA or β protein to ssDNA. This change could occur by reinstating symmetry to the Orf dimer or alterations in the order/disorder of helix E. Further work is needed to establish whether bacterial or phage recombination pathways are stimulated by Orf. Many of the structurally distinct systems for overcoming the barrier of ssDNA binding protein show species-specific interactions with the recombination enzymes they load (28, 45). The known bacterial and eukaryotic mediators are annealing proteins in their own right, so phage λ Orf and its unrelated analogue from T4 (UvsY) may be unusual amongst this group in functioning primarily in a facilitatory role.

We thank Peter McGlynn (University of Aberdeen, Aberdeen, U.K.) for the SSB overexpression construct. This work was supported by the Biotechnology and Biological Sciences Research Council, the Canadian Institutes of Health Research (CIHR), National Institutes of Health Grant GM62414 (to A.J.), the Ontario Research and Development Challenge Fund, and the United States Department of Energy, Office of Biological and Environmental Research under contract W-31-109-ENG-38. K.L.M. was supported by a CIHR Postdoctoral Fellowship.

1. Brüssow, H., Canchaya, C. & Hardt, W. D. (2004) *Microbiol. Mol. Biol. Rev.* **68,** 560–602.
2. Court, D. L., Sawitzke, J. A. & Thomason, L. C. (2002) *Annu. Rev. Genet.* **36,** 361–388.
3. Stahl, M. M., Thomason, L., Poteete, A. R., Tarkowski, T., Kuzminov, A. & Stahl, F. W. (1997) *Genetics* **147,** 961–977.
4. Kowalczykowski, S. C. (2000) *Trends Biochem. Sci.* **25,** 156–165.
5. Poteete, A. R. (2001) *FEMS Microbiol. Lett.* **201,** 9–14.
6. Little, J. W. (1967) *J. Biol. Chem.* **242,** 679–686.
7. Kmiec, E. & Holloman, W. K. (1981) *J. Biol. Chem.* **256,** 12636–12639.
8. Muniyappa, K. & Radding, C. M. (1986) *J. Biol. Chem.* **261,** 7472–7478.
9. Rybalchenko, N., Golub, E. I., Bi, B. & Radding, C. M. (2004) *Proc. Natl. Acad. Sci. USA* **101,** 17056–17060.
10. Sawitzke, J. A. & Stahl, F. W. (1992) *Genetics* **130,** 7–16.
11. Sawitzke, J. A. & Stahl, F. W. (1994) *J. Bacteriol.* **176,** 6730–6737.
12. Poteete, A. R. (2004) *J. Bacteriol.* **186,** 2699–2707.
13. Madiraju, M. V., Lavery, P. E., Kowalczykowski, S. C. & Clark, A. J. (1992) *Biochemistry* **31,** 10529–10535.
14. Wang, T. V., Chang, H. & Hung, J. (1993) *Mutat. Res.* **294,** 157–166.
15. Griffin, T. J. & Kolodner, R. D. (1990) *J. Bacteriol.* **172,** 6291–6299.
16. Webb, B. L., Cox, M. M. & Inman, R. B. (1995) *J. Biol. Chem.* **270,** 31397–31404.
17. Webb, B. L., Cox, M. M. & Inman, R. B. (1999) *J. Biol. Chem.* **274,** 15367–15374.
18. Luisi-DeLuca, C. & Kolodner, R. (1994) *J. Mol. Biol.* **236,** 124–138.
19. Luisi-DeLuca, C. (1995) *J. Bacteriol.* **177,** 566–572.
20. Kantake, N., Madiraju, M. V., Sugiyama, T. & Kowalczykowski, S. C. (2002) *Proc. Natl. Acad. Sci. USA* **99,** 15327–15332.
21. Leiros, I., Timmins, J., Hall, D. R. & McSweeney, S. (2005) *EMBO J.* **24,** 906–918.
22. Alonso, J. C., Stiege, A. C., Dobrinski, B. & Lurz, R. (1993) *J. Biol. Chem.* **268,** 1424–1429.
23. Lee, B. I., Kim, K. H., Park, S. J., Eom, S. H., Song, H. K. & Suh, S. W. (2004) *EMBO J.* **23,** 2029–2038.
24. Umezu, K. & Kolodner, R. D. (1994) *J. Biol. Chem.* **269,** 30005–30013.
25. Umezu, K., Chi, N. & Kolodner, R. D. (1993) *Proc. Natl. Acad. Sci. USA* **90,** 3875–3879.
26. Hegde, S. P., Qin, M. H., Li, X. H., Atkinson, M. A., Clark, A. J., Rajagopalan, M. & Madiraju, M. V. (1996) *Proc. Natl. Acad. Sci. USA* **93,** 14468–14473.
27. Webb, B. L., Cox, M. M. & Inman, R. B. (1997) *Cell* **91,** 347–356.
28. Morimatsu, K. & Kowalczykowski, S. C. (2003) *Mol. Cell.* **11,** 1337–1347.
29. Chow, K. H. & Courcelle, J. (2004) *J. Biol. Chem.* **279,** 3492–3496.
30. Petit, M. A. & Ehrlich, D. (2002) *EMBO J.* **21,** 3137–3147.
31. Moore, T., McGlynn, P., Ngo, H. P., Sharples, G. J. & Lloyd, R. G. (2003) *EMBO J.* **22,** 735–745.
32. Zhang, R., Andersson, C. E., Savchenko, A., Skarina, T., Evdokimova, E., Beasley, S., Arrowsmith, C. H., Edwards, A. M., Joachimiak, A. & Mowbray, S. L. (2003) *Structure (Cambridge, U.K.)* **11,** 31–42.
33. Walsh, M. A., Evans, G., Sanishvili, R., Dementieva, I. & Joachimiak, A. (1999) *Acta Crystallogr. D* **55,** 1726–1732.
34. Otwinowski, Z. & Minor, W. (1997) *Methods Enzymol.* **276,** 307–326.
35. Brunger, A. T., Adams, P. D., Clore, G. M., DeLano, W. L., Gros, P., Grosse-Kunstleve, R. W., Jiang, J. S., Kuszewski, J., Nilges, M., Pannu, N. S., *et al.* (1998) *Acta Crystallogr. D* **54,** 905–921.
36. Perrakis, A., Sixma, T. K., Wilson, K. S. & Lamzin, V. S. (1997) *Acta Crystallogr. D* **53,** 448–455.
37. Cadman, C. J. & McGlynn, P. (2004) *Nucleic Acids Res.* **32,** 6378–6387.
38. Hegde, S. P., Rajagopalan, M. & Madiraju, M. V. (1996) *J. Bacteriol.* **178,** 184–190.
39. Laskowski, R. A., MacArthur, M. W., Moss, D. S. & Thornton, J. M. (1993) *J. Appl. Crystallogr.* **26,** 283–291.
40. Holm, L. & Sander, C. (1995) *Trends Biochem. Sci.* **20,** 478–480.
41. Jones, S. & Thornton, J. M. (1996) *Proc. Natl. Acad. Sci. USA* **93,** 13–20.
42. Deo, R. C., Groft, C. M., Rajashankar, K. R. & Burley, S. K. (2002) *Cell* **108,** 71–81.
43. Wang, J., Smerdon, S. J., Jager, J., Kohlstaedt, L. A., Rice, P. A., Friedman, J. M. & Steitz, T. A. (1994) *Proc. Natl. Acad. Sci. USA* **91,** 7242–7246.
44. Ellis, H. M., Yu, D., DiTizio, T. & Court, D. L. (2001) *Proc. Natl. Acad. Sci. USA* **98,** 6742–6746.
45. Beernink, H. T. & Morrical, S. W. (1999) *Trends Biochem. Sci.* **24,** 385–389.